Supporting Information

Icosahedral Platinum Alloy Nanocrystals with Enhanced Electrocatalytic Activities

*Jianbo Wu,[1,2] Liang Qi,[3] Hongjun You,[1] Adam Gross,[1] Ju Li,[3] Hong Yang[1,2]**

1 Department of Chemical Engineering, University of Rochester, Rochester, New York 14627.

2 Department of Chemical & Biomolecular Engineering, University of Illinois, at Urbana-Champaign, 600 S. Mathews Ave, Urbana, Illinois 61801.

3 Department of Nuclear Science and Engineering and Department of Materials Science and Engineering, Massachusetts Institute of Technology, Cambridge, Massachusetts, 02139.

*Corresponding author

E-mail: hy66@illinois.edu

Telephone: (217) 244-6730

Experimental Section

Synthesis of Pt_3Ni Icosahedral Nanoparticles. To synthesize Pt_3Ni icosahedral nanocrystals, a solution of 8 mg (0.017 mmol) of platinum acetylacetonate [$Pt(acac)_2$], 12.9 mg (0.05 mmol) of nickel acetylacetonate [$Ni(acac)_2$], 9 mL of oleylamine (OAm) and 1 mL of oleic acid (OA) was mixed in a 25 mL three-neck round bottom flask immersed in an oil bath at 130 °C. The reaction mixture turned into a transparent yellowish solution at this temperature after 2 min. The flask was then transferred to a second oil bath at 210 °C under a flow of carbon monoxide (CO) gas (C.P. Grade, Airgas). The typical flow rate of CO gas was set at 190 cm^3/min and the reaction time was 30 min. The PtAu icosahedral nanocrystals was obtained with 20.0 mg (or 0.050 mmol) of $Pt(acac)_2$ and 19.0 mg (or 0.050 mmol) of $HAuCl_4$, following the same procedure for making Pt_3Ni icosahedral nanocrystals. For Pt-Pd alloys, 20 mg of $Pt(acac)_2$ and 4.0 mg (or 0.017mmol) of palladium acetylacetonate [$Pd(acac)_2$] were used to make Pt_3Pd icosahedral nanocrystals, and 20 mg of $Pt(acac)_2$ and 11.4 of mg $Pd(acac)_2$ for PtPd icosahedral nanocrystals, together with 9 mL of OAm and 1 mL of diphenyl ether. The rest of steps followed the procedures for the synthesis of Pt_3Ni icosahedral nanocrystals. The solid products were washed and separated by dispersing the reaction mixture in 2 mL of chroloform and 10 mL of ethanol, followed by centrifugation at 5000 rpm for 5 min. This procedure was repeated three times. The final products were dispersed in chroloform for further characterization.

Preparation of Carbon-Supported Catalysts. Carbon black (Vulcan XC-72) was used as support for making platinum nickel catalysts (Pt_3Ni/C). In a standard preparation, carbon black particles were dispersed in chroloform and sonicated for 1 h. A designed amount of platinum nickel nanoparticles were added to this dispersion at the nanoparticle-to-carbon-black mass ratio of 20:80. This mixture was further sonicated for 30 min and stirred overnight. The resultant solids were precipitated out by centrifugation and dried under an argon stream. The solid product was then re-dispersed in n-butylamine at a concentration of 0.5 mg-catalyst/mL. The mixture was kept under stirring for 3 days and then collected using a centrifuge at a rate of 5000 rpm for 5 min. The precipitate was re-dispersed in 10 mL methanol by sonicating for 15 min and then separated by centrifugation. This procedure was repeated three times. The final samples were dispersed in ethanol for further characterization.

Characterization. Transmission electron microscopy (TEM) and high-resolution transmission electron microscopy (HR-TEM) micrographs were taken on a FEI TECNAI F-20 field emission microscope at an accelerating voltage of 200 kV. Scanning transmission electron microscopy (STEM) micrographs and elemental maps were carried out using the high-angle annular dark field (HAADF) mode on the same microscope. Energy dispersive X-ray (EDX) analysis was carried out on a field emission scanning electron microscope (FE-SEM, Zeiss-Leo DSM982) equipped with an EDAX detector. Powder X-ray diffraction (PXRD) patterns were recorded using a Philips MPD diffractometer with a Cu Kα X-ray source (λ=1.5405 Å).

Electrochemical Measurement. A three-electrode cell was used to measure the electrochemical properties. The working electrode was a glassy-carbon rotating disk electrode (RDE) (area: 0.196 cm^2). A 1 cm^2 platinum foil was used as the counter electrode and a HydroFlex hydrogen electrode was used as the reference, which was placed in a separate compartment. Hydrogen evolution reaction (HER) was used to calibrate this hydrogen electrode before the tests. All

potentials were referenced to the reversible hydrogen electrode (RHE). The electrolyte was 0.1 M $HClO_4$, diluted from 70% double-distilled perchloric acid (GFS Chemicals, USA) with Millipore® ultra pure water. The mass of metal in each Pt_3Ni/C catalyst was determined by thermogravimetric analysis (TGA) using an SDT-Q600 TGA/DSC system from TA Instruments at a ramp rate of 10 °C/min to 600 °C in air followed by annealing at 600 °C for 30 min under a forming gas of 5% hydrogen in argon at a flow rate of 50 ml/min. To prepare the working electrode, 5 mg of the Pt_3Ni/C catalyst (20% based on the weight of alloy nanocrystals) was dispersed in 10 mL of a mixed solvent and sonicated for 5 min. The solvent contained a mixture of de-ionized water, isopropanol, and 5% Nafion at the volumetric ratio of 8:2:0.05. 20 μL of the suspension was added onto the RDE by a pipette and dried in air. The loading amount of Pt_3Ni alloy nanocatalysts on the RDE was determined to be 9.3 $\mu g_{Pt}/cm^2$. The electrochemical active surface area (ECSA) was determined from the cyclic voltammetry (CV) curves. The amount of charges due to the adsorption of hydrogen species was obtained by integrating the area between 0.05 and 0.4 V. The CV measurement was carried in argon-saturated 0.1 M $HClO_4$ solution at room temperature with a scan rate of 50 mV/s. Oxygen reduction reaction (ORR) activities were determined in a 0.1 M $HClO_4$ solution which was purged with oxygen for 30 min prior to, and during testing. The scan rate for ORR measurement was set at 10 mV/s in the positive direction. Data were used without iR-drop correction. For comparison, Pt/C (E-TEK, 20 wt%Pt on Vulcan carbon) was used as the reference. The same procedure as described above was used to conduct the electrochemical measurement, except that the Pt loading was controlled at 11 $\mu g_{Pt}/cm^2$.

Density Functional Theory (DFT) Calculations. All DFT calculations are performed by using the Vienna *ab initio* simulation package (VASP).[1] We use projector augmented wave (PAW)[2] potentials with Perdew-Burke-Ernzerhof (PBE) exchange-correlation functional[3] in none-spin-polarized conditions. Partial occupancies of eigenstates are determined by first-order Methfessel-Paxton smearing of $\sigma = 0.2$ eV. Cut-off energy for plane wave basis is 400 eV. Just the gamma point is used for Brillouin-zone integration because of the isolated cluster configuration. The method to generate atomic coordinates of icosahedral cluster is described in previous literature.[4] The projected density of states (DOS) of individual atom is obtained with LORBIT = 12, from which the d-band center is calculated. The adsorption configurations of hydroxyl (OH) on the edge and {111} facet of Pt icosahedral and octahedral clusters are shown in Figure S16.

The coordinate number (CN) of atoms on the {111} facets of icosahedral and octahedral cluster are the same (CN=9). However, the tensile/compressive strain on icosahedral/octahedral cluster shifts up/down d-band center of surface electrons, as shown in Figure S17, so the adsorption energy of OH on {111} facet of Pt icosahedral cluster in Figure S16 is 0.26 eV stronger than that on Pt octahedral cluster. On the other hand, CN of Pt atom on the edge of icosahedral and octahedral cluster is 8 and 7, respectively, so it was expected that the adsorption energy of OH on the edge of icosahedral cluster should be much lower than its counterpart on octahedral cluster because of the change of bond saturation. However, due to the same strain effect, such difference is largely cancelled off. Thus, OH adsorption energy on the edge of Pt icosahedral cluster is only 0.05 eV weaker than its counterpart on octahedral cluster. In summary, because of geometrical and its corresponding strain effects, icosahedral and octahedral clusters have similar adsorption properties on the edges, but different properties on the {111} facets.

We also make Pt_3Ni icosahedral (309 atoms) and octahedral (146 atoms) clusters and use DFT

calculations to investigate their electronic structures. Previous studies suggested that it is pure Pt on top layer of real Pt_3Ni alloy nanoparticles[5]. However, because ~50% atoms are on the top layer of the clusters used in our DFT calculations, we randomly put 25% Ni atoms in these clusters to keep the Pt:Ni atomic ratio as 3:1, as shown in Figure S18. The projected DOS of each Pt atom on all {111} facets (CN=9) is calculated for both clusters and the results are plotted in Figure S19. Similar with pure Pt, the average d-band center of Pt_3Ni icosahedral cluster is 0.26 eV higher than that of Pt_3Ni octahedral cluster, so on average the adsorption energies of ORR intermediates on {111} facet of Pt_3Ni icosahedral cluster should be stronger than those on Pt_3Ni octahedral cluster.

Molecular Dynamics (MD) Simulations. To obtain the surface strain of nanoparticles, MD simulations were performed by LAMMPS with EAM interatomic potential of Pt.[6] Pure Pt icosahedral and octahedral nanoparticles with diameter = 10 nm are built based on previous literature.[4] To obtain the equilibrium configurations, conjugated gradient (CG) minimization is applied to the whole nanoparticles, followed by MD simulations at 50 K for 100 picoseconds. Finally, the equilibrium configuration of nanoparticles is obtained by repeating the initial CG minimization procedure. The characteristic surface bond length of individual surface atom is calculated by averaging the lengths of all its bonds connecting to nearest-neighbor surface atoms, from which the surface strain is calculated based on the equilibrium bond length (2.772 Å) in bulk lattice of this Pt EAM potential.[6]

We also investigate the surface strain on alloy icosahedral and octahedral nanoparticles with diameter = 10 nm. Since there is no good classical MD potential for Pt-Ni system available, we chose Al-Cu potential instead[7]. This approach is reasonable because we only consider the strain instead of chemical information and Al-Cu system has similar structure as Pt-Ni. For instance, Pt and Ni have FCC lattice with lattice constant 3.92 Å and 3.52 Å, respectively; Al and Cu also have FCC lattice with lattice constant 4.05 Å and 3.62 Å, respectively. In both cases we add smaller atoms (Ni/Cu) into lattice of larger atoms (Pt/Al). Thus both pure Al nanoparticles and Al_3Cu nanoparticles with pure Al top layer are constructed to model the observed structure of pure Pt on the top layer of Pt_3Ni alloy nanoparticles[5].

The surface strain distributions on these bimetallic alloy nanoparticles are shown in Figure S20 and the histograms of surface strain are shown in Figure S21. First, like pure Pt nanoparticles, there is averagely +1.9% tensile strain on {111} facets of pure Al icosahedral nanoparticles and averagely -0.7% compressive strain on pure Al octahedral nanoparticles. When 25% Cu atoms are randomly added into the bulk of these nanoparticles, the strain of Al surface layer decreases in both nanoparticles because of the smaller volume of Cu atoms, which should increase the stabilities of icosahedral nanoparticles under large tensile stress. Meanwhile, the same strain difference still exists: there is averagely -0.9% compressive strain on {111} facets of Al_3Cu icosahedral nanoparticles and averagely -2.7% compressive strain on Al_3Cu octahedral nanoparticles. Here surface strain is calculated based on the lattice constant of pure Al, thus it should be tensile strain for Al_3Cu icosahedral nanoparticles if the lattice constant of Al_3Cu is used as the reference. The results confirm that no matter which strain reference is applied, there is a 2%~3% strain difference for {111} facets between icosahedral and octahedral nanoparticles. This is a general phenomenon and independent of materials, which should result in differences of d-band center and adsorption energy.

References:

1. Kresse, G.; Furthmuller J. *Phys. Rev. B* **1996**, *54*, 11169-11186.
2. Blochl, P. E. *Phys. Rev. B* **1994,** *50,* 17953-17979.
3. Perdew, J. P.; Burke, K.; Ernzerhof, M. *Phys. Rev. Lett.* **1996**, ***77***, 3865-3868.
4. Glasner, D.; Frenkel, A. I. *Geometrical characteristics of regular polyhedra: Application to EXAFS studies of nanoclusters*, in *X-Ray Absorption Fine Structure-XAFS13*, Hedman, B. P. P. (Ed), **2007**, p. 746-748.
5. Stamenkovic, V. R.; Fowler, B.; Mun, B. S.; Wang, G. F.; Ross, P. N.; Lucas, C. A.;Markovic, N. M. *Science* **2007**, *315,* 493-497.
6. Foiles, S. M.; Baskes, M. I.; Daw, M.S. *Phys. Rev. B* **1986**, *33,* 7983-7991.
7. Cai, J.; Ye, Y. Y. *Phys. Rev. B* **1996,** *54*, 8398-8410.

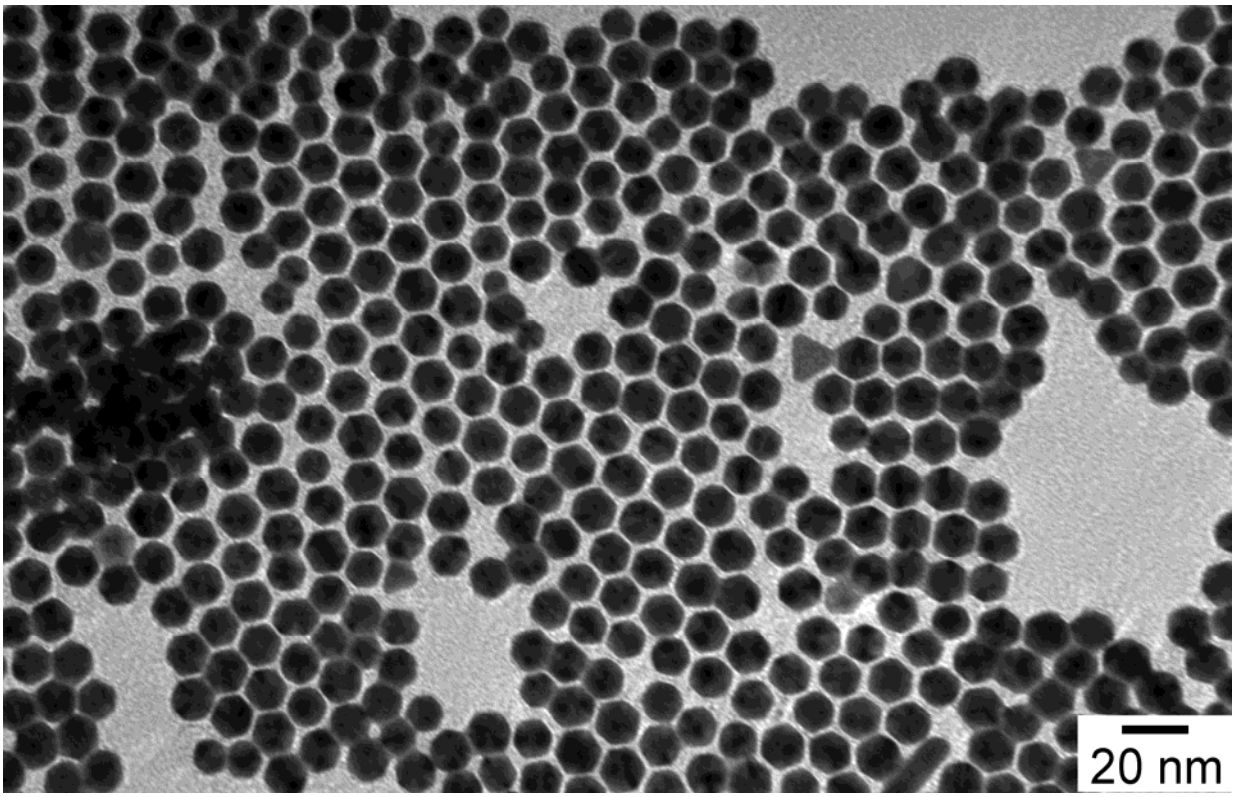

Figure S1. TEM micrograph of Pt_3Ni icosahedral nanocrystals in large area.

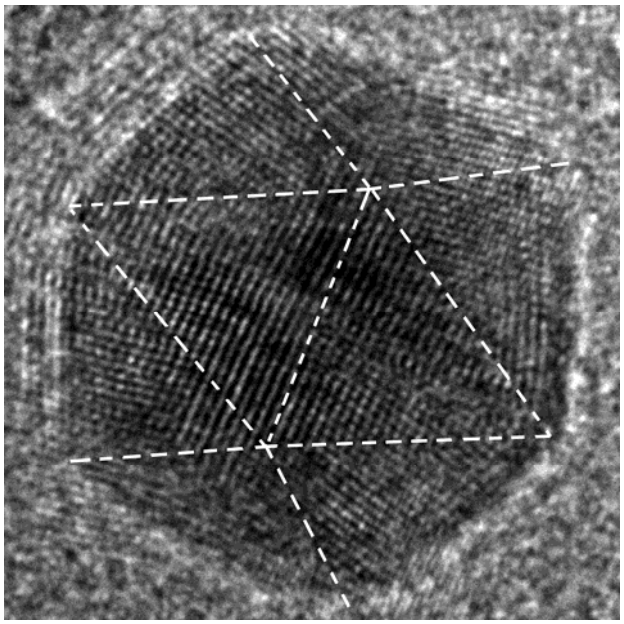

Figure S2, HRTEM micrograph of an individual icosahedral Pt_3Ni nanocrystal, showing the twin boundaries of five-fold symmetry.

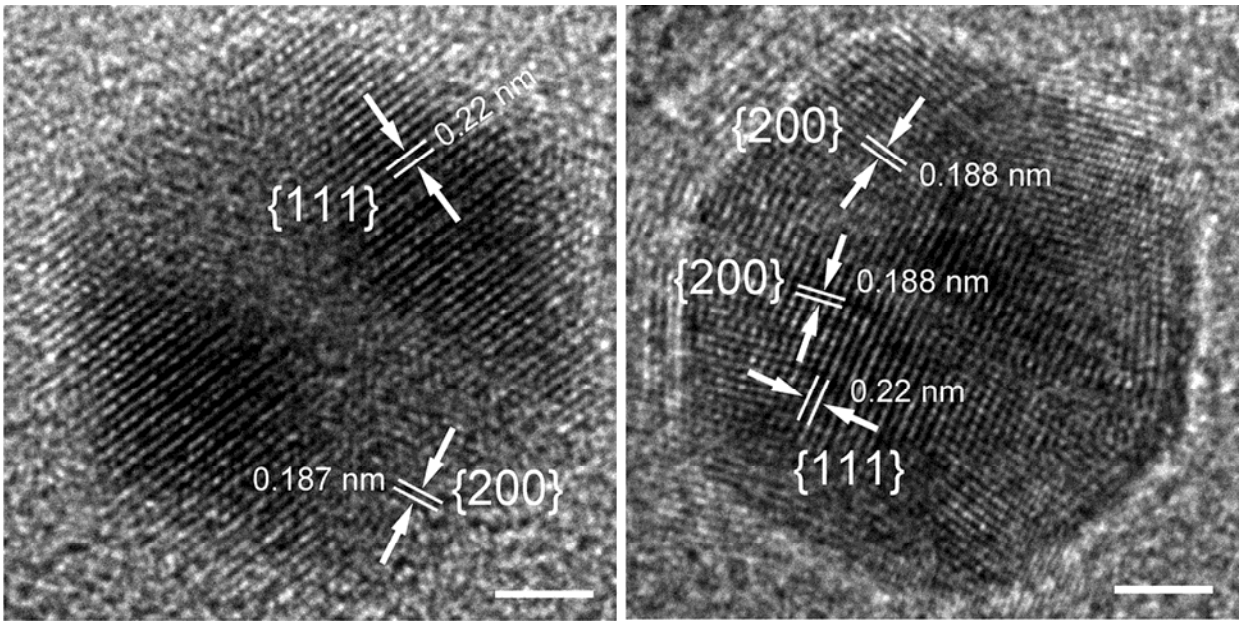

Figure S3. HRTEM macrographs of icosahedral Pt_3Ni nanocrystals at two different imaging directions (the scale bars correspond to 2 nm).

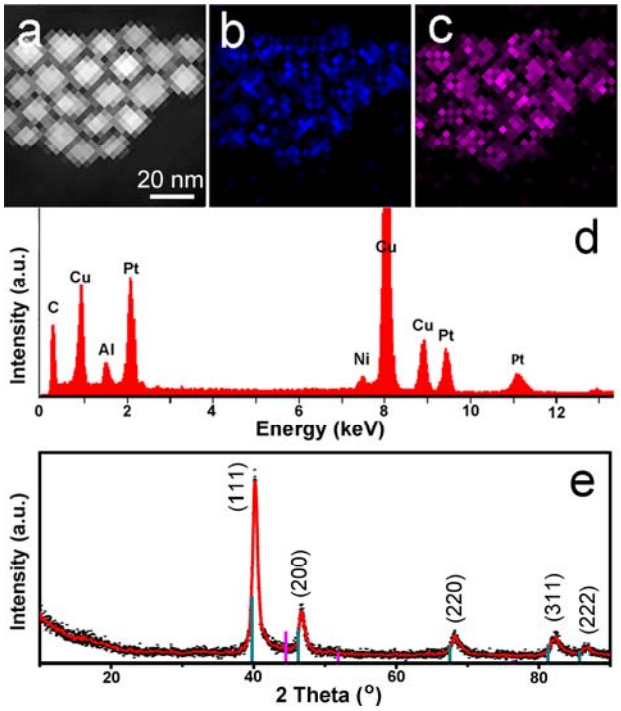

Figure S4. (a) HAADF-STEM image, its corresponding (b) Pt and (c) Ni elemental maps, (d) EDX spectrum and (e) XRD pattern of Pt_3Ni alloy icosahedral nanocrystals (color code: blue: Pt, purple: Ni).

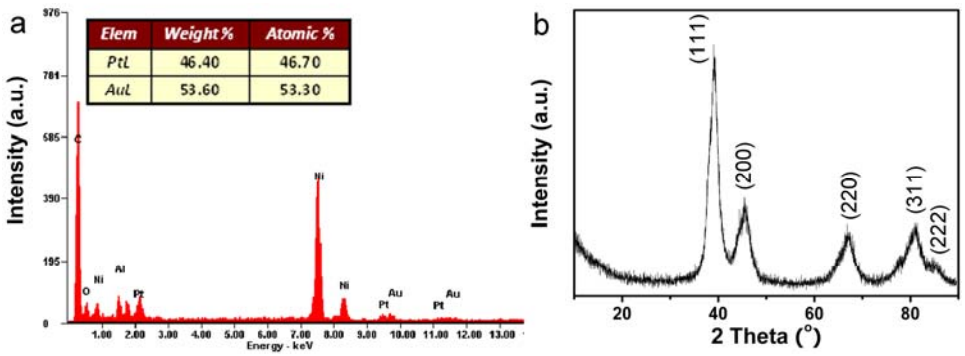

Figure S5. (a) SEM-EDX spectrum and (b) XRD pattern of PtAu icosahedral nanocrystals.

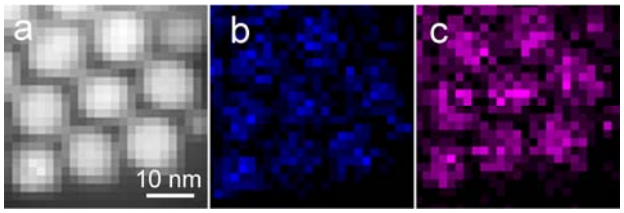

Figure S6. (a) STEM image and its corresponding elemental maps of (b) Pt and (c) Au of the PtAu nanocrystals.

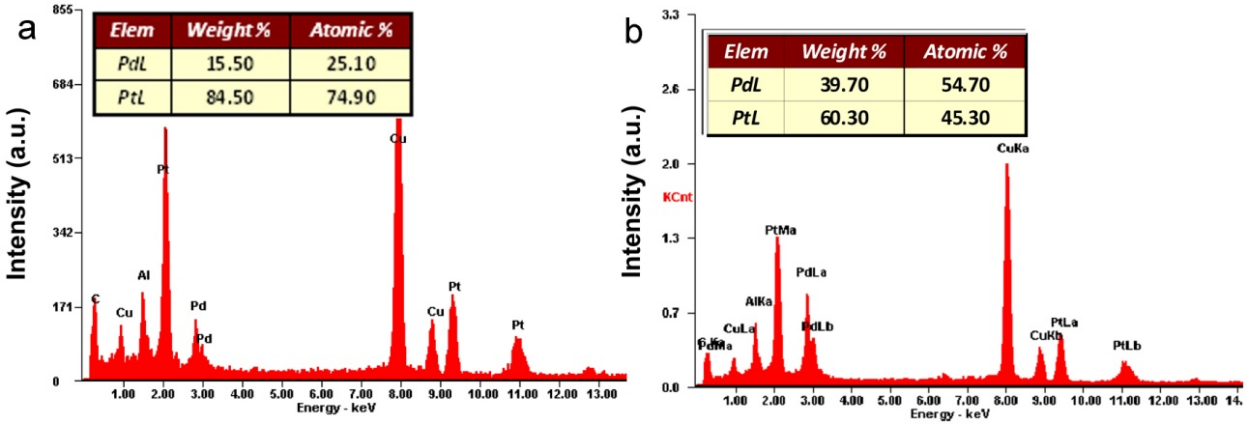

Figure S7. SEM-EDX spectra of (a) Pt_3Pd and (b) PtPd icosahedral nanocrystals, respectively.

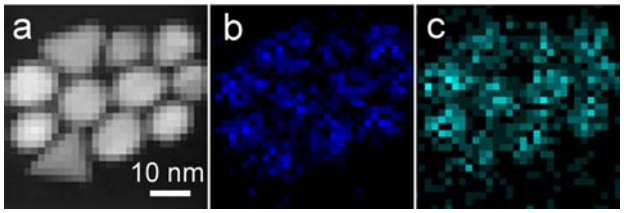

Figure S8. (a) STEM image and its corresponding elemental maps of (b) Pt and (c) Pd of the Pt_3Pd nanocrystals.

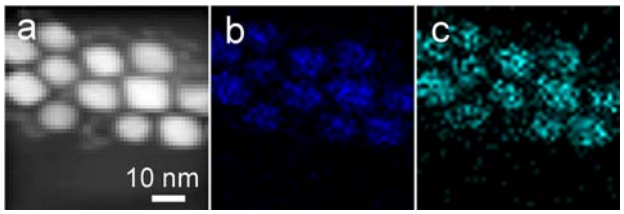

Figure S9. (a) STEM image and its corresponding elemental maps of (b) Pt and (c) Pd of the PtPd nanocrystals.

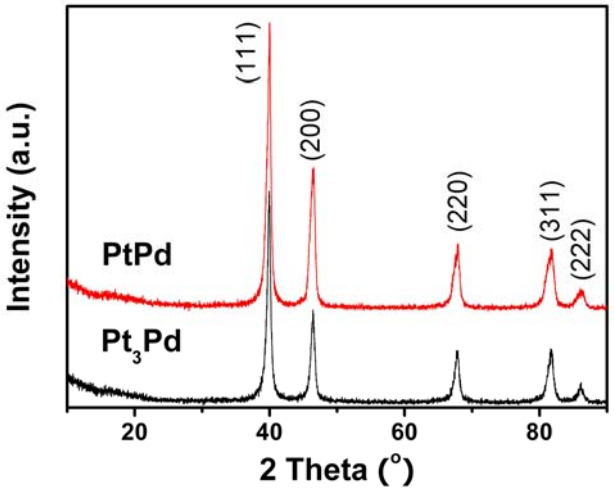

Figure S10. XRD patterns of Pt_3Pd and PtPd icosahedral nanocrystals, respectively.

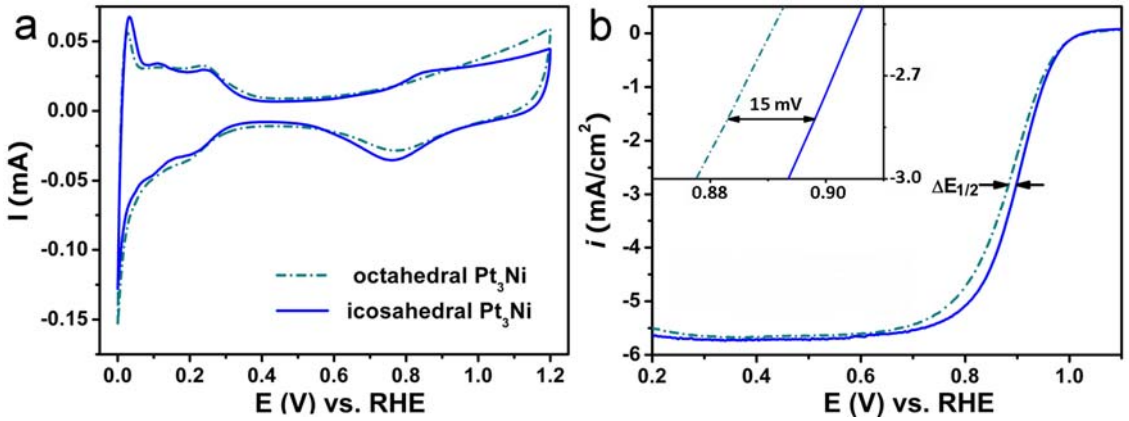

Figure S11. (a) CV curves and (b) ORR polarization of the Pt_3Ni octahedral and icosahedral nanocrystal catalysts. Inset in (b) shows the half-wave potential.

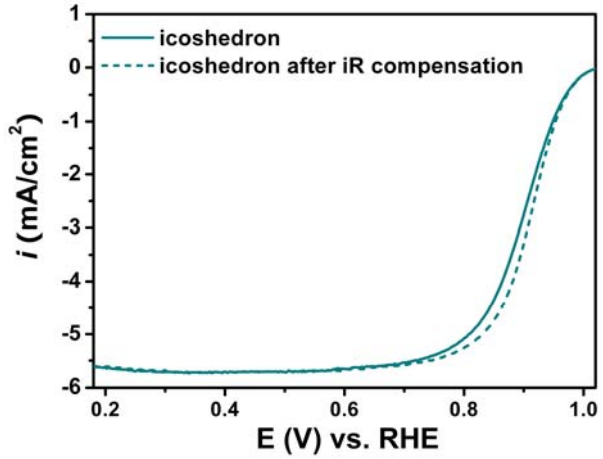

Figure S12. ORR polarization of octahedral Pt_3Ni catalysts without (solid line) and with (dash line) iR compensation, respectively.

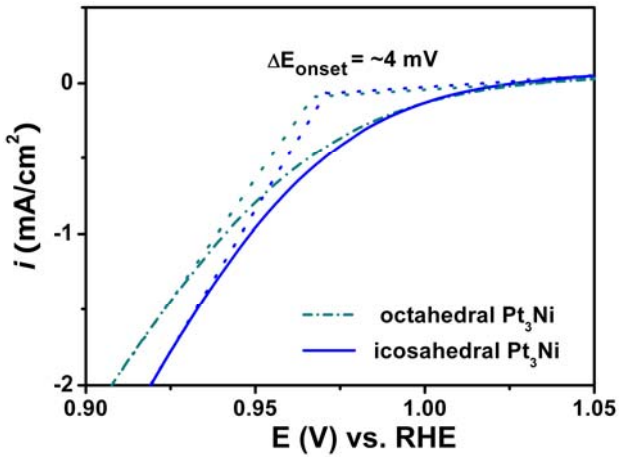

Figure S13. Onset potentials of the Pt_3Ni octahedral and icosahedral nanocrystal catalysts.

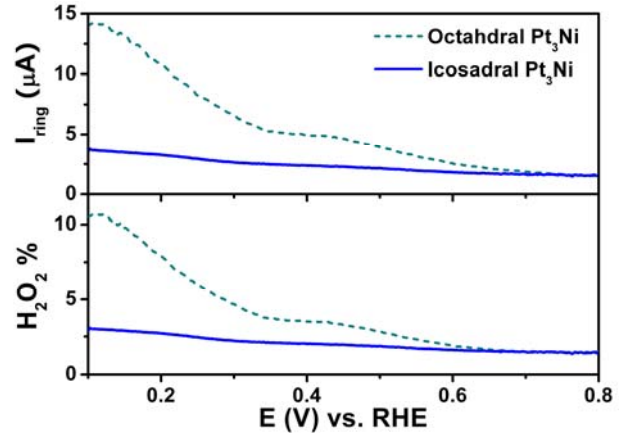

Figure S14. Ring currents corresponding to H_2O_2 oxidation (E_{ring} = 1.2 V vs RHE) and the corresponding calculated amount of H_2O_2, formed during the oxygen reduction reaction on octahedral and icosahedral Pt_3Ni/Vulcan XC-72 catalysts. These tests were carried out in 0.1 M $HClO_4$ solution at a rotating rate of 1600 rpm.

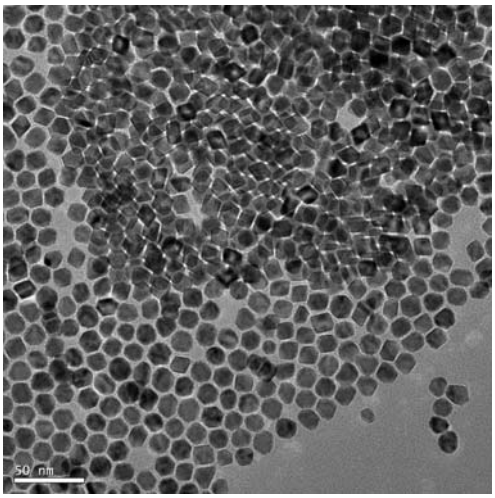

Figure S15. TEM micrograph of 12 nm octahedral Pt_3Ni nanoparticles

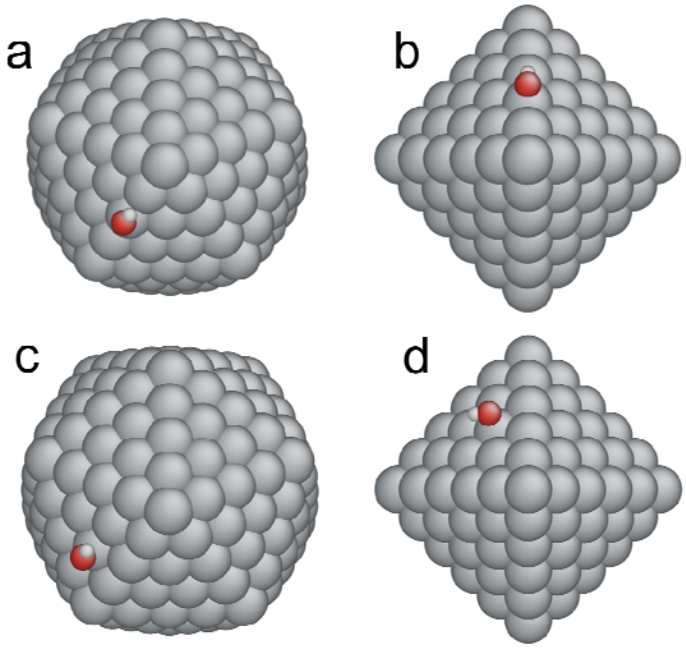

Figure S16. Atomic structure of (a) Pt icosahedral cluster of 309 atoms and (b) Pt octahedral cluster of 146 atoms, where there is OH adsorbed on the edge between two {111} facets. (c) and (d): Atomic structure of the same Pt (c) icosahedral and (d) octahedral clusters with OH adsorbed on {111} facets.

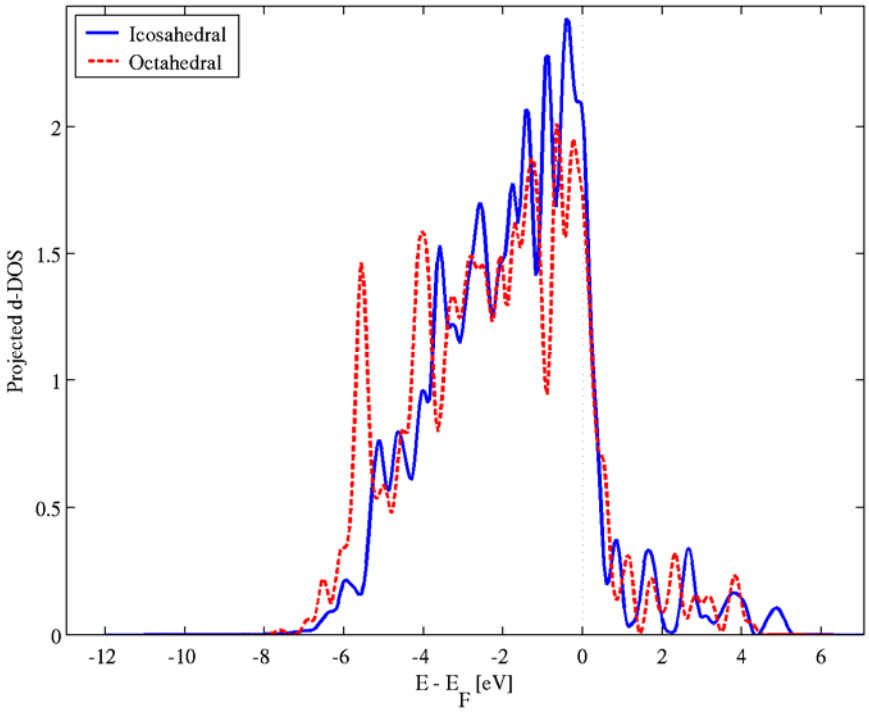

Figure S17. Projected d-DOS of Pt atoms on the {111} facets (CN = 9) of icosahedral and octahedral clusters shown in Figure S15. E_F is Fermi energy. The d-band center of Pt atoms on the {111} facets of icosahedral cluster is 0.36 eV higher than that of octahedral cluster.

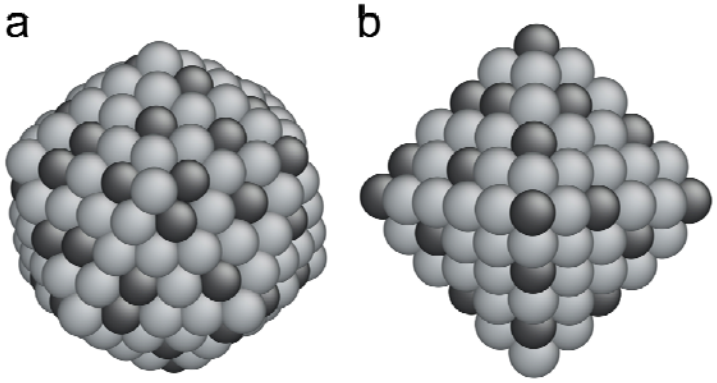

Figure S18. Atomic structure of Pt_3Ni (a) icosahedral cluster of 309 atoms and (b) Pt_3Ni octahedral cluster of 146 atoms. Ni atoms are randomly distributed. Color code: grey, Pt atom and black, Ni atom.

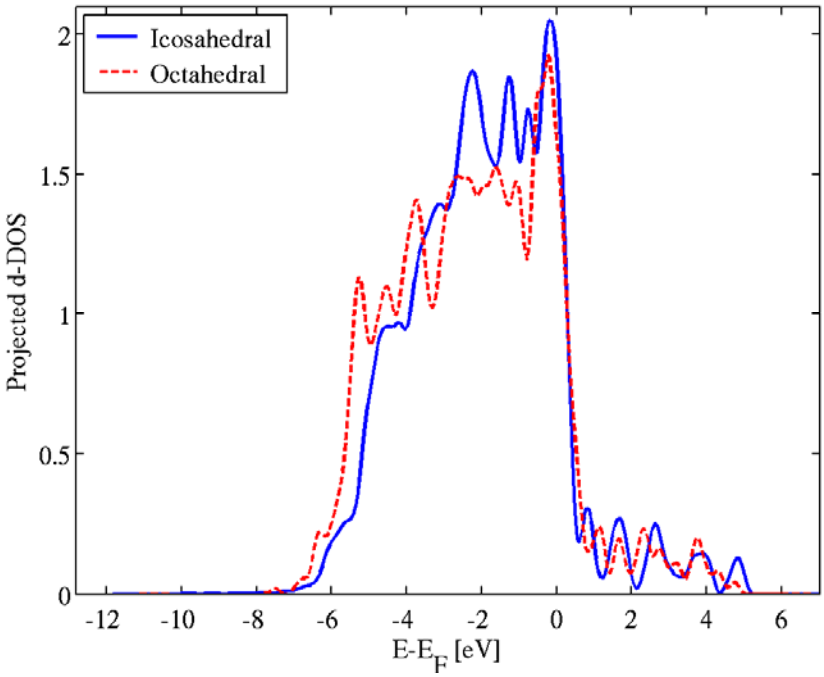

Figure S19. Average projected d-DOS of Pt atoms on the {111} facets (CN = 9) of icosahedral and octahedral clusters shown in Figure S17. The average d-band center of Pt atoms on the {111} facets of icosahedral cluster is 0.26 eV higher than that of octahedral cluster.

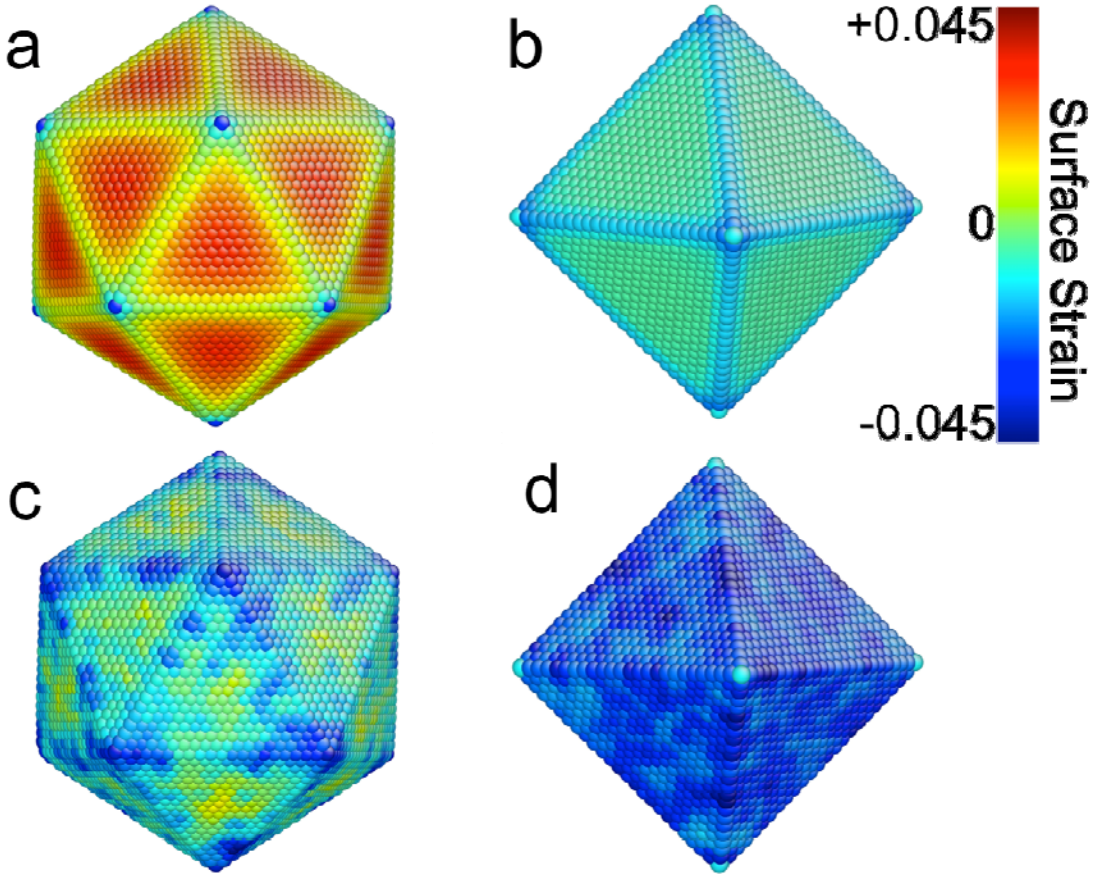

Figure S20. Surface strain on nanoparticles with diameters of 10 nm: (a) Al icosahedral, (b) Al octahedral, (c) Al_3Cu icosahedral with pure Al as top layer, and (d) Al_3Cu octahedral with pure Al as top layer. All surface strain is calculated based on the lattice constant of pure Al.

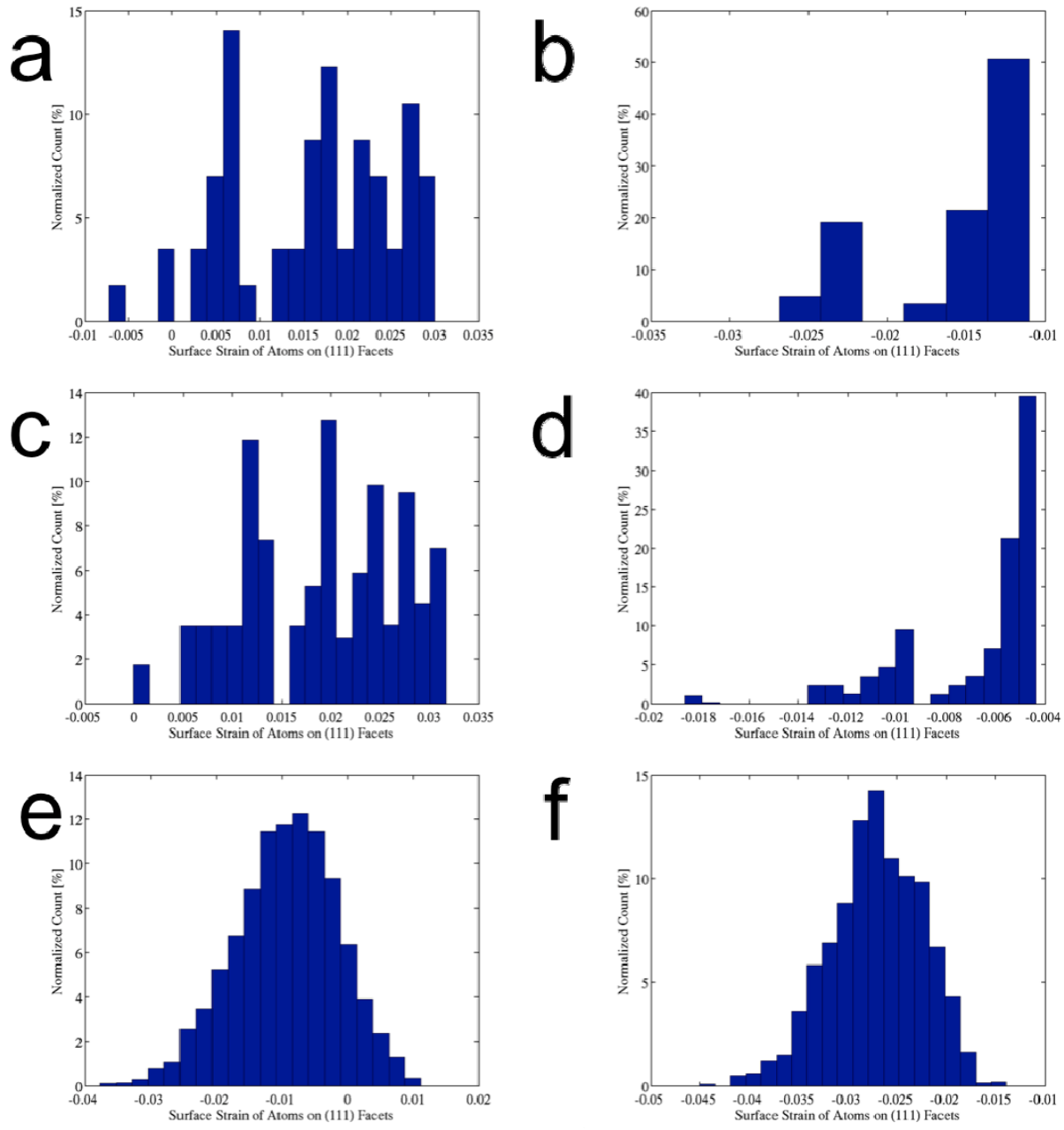

Figure S21. Histogram of surface strain for all atoms on {111} facets (CN = 9) of nanoparticles with size of ~10 nm: (a) Pt icosahedral, (b) Pt octahedral, (c) Al icosahedral, (d) Al octahedral, and (e) Al_3Cu icosahedral with pure Al as top layer, and (f) Al_3Cu octahedral with pure Al as top layer.

Table S1. ECSA, Mass- and Area- Specific ORR Activities of Icosahedral Pt_3Ni Catalysts *

	i_s (mA/cm^2_{Pt})	i_m ($mA/\mu g_{Pt}$)
as measured	1.83	0.62
after iR compensation	2.78	0.94

*: The activity was measured at 0.9 V (vs. RHE). ECSA value is 33.9 m^2/g_{Pt} for both cases.